

## Corrosion of alloys in high temperature molten-salt heat transfer fluids with air as the cover gas

Tianle Liu, Xinhai Xu\*, Wenrui Liu, Xiaoru Zhuang

School of Mechanical Engineering and Automation, Harbin Institute of Technology, Shenzhen 518055, China



### ARTICLE INFO

**Keywords:**  
Corrosion  
Ni-based alloy  
Heat transfer fluid  
Molten-salt  
High temperature

### ABSTRACT

The state-of-the-art concentrated solar power tower technology requires novel heat transfer fluids which can operate at a temperature as high as 700 °C. Several molten eutectic salt mixtures are promising heat transfer fluid candidates because they are thermally stable at such high temperature and have good thermophysical properties. However, their corrosion properties to alloys are not investigated thoroughly in the literature. Molten salts usually have high corrosion to alloys, which is a critical issue since the piping and containing materials of the heat transfer fluid in a solar power plant are generally alloys. In this study, the corrosion of three eutectic mixtures including NaCl-KCl-ZnCl<sub>2</sub>, Li<sub>2</sub>CO<sub>3</sub>-Na<sub>2</sub>CO<sub>3</sub>-K<sub>2</sub>CO<sub>3</sub> and LiF-Na<sub>2</sub>CO<sub>3</sub>-K<sub>2</sub>CO<sub>3</sub> to different alloys were experimentally studied at isothermal condition of 700 °C in contact with air. Alloys tested were stainless steel 316 (SS316), Hastelloy C276 (C276), Inconel 625 (In625) and 718 (In718). Scanning electron microscope (SEM), energy dispersive spectroscopy (EDS) and X-ray diffraction (XRD) techniques were employed to characterize the coupon surfaces after corrosion tests. Results show that all the alloys have corrosion rates higher than 450 µm/year immersed in the NaKZn chloride-salt. Therefore, the NaKZn chloride-salt is not applicable as a heat transfer fluid if air cannot be evacuated. C276 immersed in the LiNaK carbonate-salt and In718 immersed in the LiF-NaK carbonate-salt may form protective compact layers on the alloy surfaces to resist corrosion. However, the high cost of lithium salts is another major obstacle to commercialize heat transfer fluids.

### 1. Introduction

Concentrated solar power (CSP) technology can utilize renewable solar energy to produce clean electricity. It concentrates solar irradiation using lenses or mirrors onto the receiver, where the concentrated heat energy is collected by the heat transfer fluid (HTF). The HTF can release heat in a heat exchanger generating high temperature steam to drive the traditional steam turbine (Zhang et al., 2013; Vignarooban et al., 2015). The three most significant sub-systems of a CSP plant are the solar collection system, the HTF circulation system and the power block. Molten-salts have been widely used in commercial CSP plants as the HTF because of their high thermally stable temperature and good thermophysical properties (Peng et al., 2010). The thermal energy storage (TES) system is also critical because it can ensure delivery of dispatchable power on demands regardless of time or weather (Xu et al., 2016). Except for working as the energy carrier in the circulation system, molten-salts can be used as the heat storage medium as well due to their high heat capacity.

Because a huge amount of HTF is required to transfer and store heat in a CSP plant, it is important to employ the most appropriate material

as the HTF considering the operating conditions for the sake of minimizing the HTF cost and maximizing the system efficiency (Xu et al., 2017). The costs of the HTF circulation system and the TES system are reported to contribute as much as 20% of the total capital investment for a CSP plant (Zhao et al., 2017; Zhu et al., 2015). High HTF operating temperature in a CSP plant is beneficial because it can improve the heat to electricity conversion efficiency. In 2014, U.S. Department of Energy (DOE) announced the target to investigate receivers with the HTF exit temperature of 720 °C in the SunShot program, which suggests that the appropriate HTF candidates must be thermally stable at temperatures up to 720 °C. To the authors' best knowledge, only a few eutectic salt mixtures reported in the literature can remain stable at the temperature around 700 °C, which are the NaCl-KCl-ZnCl<sub>2</sub> ternary chloride-salt mixture (Li et al., 2016), the Li<sub>2</sub>CO<sub>3</sub>-Na<sub>2</sub>CO<sub>3</sub>-K<sub>2</sub>CO<sub>3</sub> ternary carbonate-salt mixture (Olivares et al., 2012), and the LiF-Na<sub>2</sub>CO<sub>3</sub>-K<sub>2</sub>CO<sub>3</sub> ternary fluoride-carbonate-salt mixture (Wang et al., 2015). Even though these salt mixtures show promising thermophysical properties (Li et al., 2016; Olivares et al., 2012; Wang et al., 2015; Ejima et al., 1987; An et al., 2016), their corrosion properties to different alloys have not been thoroughly investigated. However, low corrosion to metal alloys is a

\* Corresponding author.

E-mail address: [xuxinbai@hit.edu.cn](mailto:xuxinbai@hit.edu.cn) (X. Xu).

**Table 1**

Thermophysical properties of the tested eutectic salt mixtures.

Eutectic salt mixture	Melting point (°C)	Thermal stable temperature (°C)	Thermal conductivity (W/m·K)	Heat capacity (J/g·K)
NaCl-KCl-ZnCl <sub>2</sub>	229	> 800	~0.3	0.9
Li <sub>2</sub> CO <sub>3</sub> -Na <sub>2</sub> CO <sub>3</sub> -K <sub>2</sub> CO <sub>3</sub>	400	660–710	~0.5	1.6
LiF-Na <sub>2</sub> CO <sub>3</sub> -K <sub>2</sub> CO <sub>3</sub>	420	797	~1.1	1.9

**Table 2**

Compositions of the tested alloys.

Alloys	Compositions (wt%)									
	Fe	Ni	Co	Cr	Mo	W	Ta	Nb	V	Ti
SS316	62–69 <sup>c</sup>	9.5–13	–	16–18.5	2–2.5	–	–	–	–	–
C276	4–7	51–59 <sup>c</sup>	2.5 <sup>a</sup>	14.5–16.5	15–17	3–4.5	–	–	0.35 <sup>a</sup>	–
In 625	5.0 <sup>a</sup>	58 <sup>b</sup>	1.0 <sup>a</sup>	20–23	8–10	–	0.05 <sup>a</sup>	3.15–4.15	–	0.4 <sup>a</sup>
In 718	11–22 <sup>c</sup>	50–55	1.0 <sup>a</sup>	17–21	2.8–3.3	–	0.05 <sup>a</sup>	4.75–5.5	–	0.65–1.15

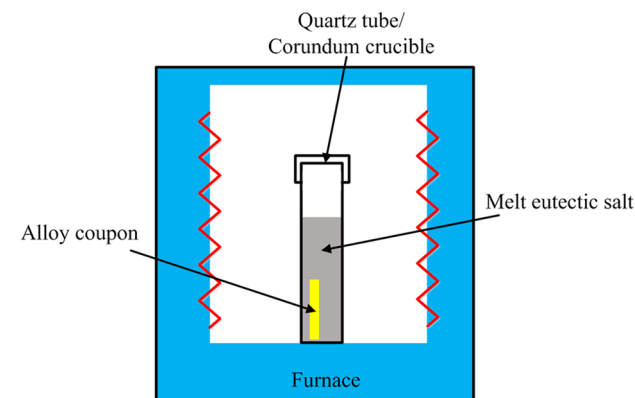
<sup>a</sup> Maximum.<sup>b</sup> Minimum.<sup>c</sup> Balanced.**Table 3**

Information of the used salts.

Salts	Chemical supplier	Purity
NaCl	Shanghai Macklin Biochemical Co., Ltd	AR, 99.5%
KCl	Shanghai Macklin Biochemical Co., Ltd	AR, 99.5%
ZnCl <sub>2</sub>	Shanghai Macklin Biochemical Co., Ltd	AR, 98.0%
Na <sub>2</sub> CO <sub>3</sub>	Damao Chemical Reagent Factory, Tianjin, China	AR, 99.8%
K <sub>2</sub> CO <sub>3</sub>	Damao Chemical Reagent Factory, Tianjin, China	AR, 99.0%
LiF	Shanghai Macklin Biochemical Co., Ltd	AR, 99.0%
Li <sub>2</sub> CO <sub>3</sub>	Shanghai Macklin Biochemical Co., Ltd	AR, 99.5%

key factor for the practical application of a HTF candidate, especially for molten-salt mixtures. Molten-salt mixtures usually have relatively high corrosion to alloys at high operating temperatures, which is unacceptable in a CSP plant since the containing and piping materials contacting the HTF are generally alloys (Bauer et al., 2013).

The most commonly used molten-salt mixture in commercial CSP plants is a binary eutectic mixture of NaNO<sub>3</sub>-KNO<sub>3</sub> (60–40 wt%), namely ‘Solar Salt’ (Kuravi et al., 2013). Goods and Bradshaw (2004) studied the corrosion of two stainless steels (SS304 and SS316) immersed in the Solar Salt at 570 °C in air. The corrosion rates were measured in immersion tests for 7000 h. The results show that the corrosion rates of SS304 and SS316 both fall in the range of 6–15 µm/year. SEM and XRD results show that the oxides formed on the stainless steel surfaces are primarily iron-chromium spinel, iron oxides, and sodium ferrite (Goods et al., 1994). Fernandez et al. (2014) employed the immersion method to test the corrosion rate of an alumina-forming austenitic stainless steel OC-4 and a low-Cr (~2%) alloy steel T22 in the Solar Salt in air for 2000 h. The T22 shows great mass gain after immersion and the SEM image clearly shows the formation of porous oxide layers with cracks in its surface. In contrast, the mass gain of the OC-4 is almost negligible and only due to salt deposition. XRD also confirms that no corrosion product formed on the OC-4 specimen. The authors concluded that the good corrosion resistance of the OC-4 was because of the high content of Cr (~14%). The Sandia National Laboratories (SNL) tested the corrosion rates of SS321, SS347 and two nickel-based alloys In625 and HA230 in the Solar Salt at 680 °C in air (Kruizenga et al., 2013). The tested temperature already exceeds the thermally stable temperature of the Solar Salt (600 °C). Immersion test results indicate the corrosion rates of SS321, SS347, In625 and HA230

**Fig. 1.** Schematic of the immersion test system.

are 460, 447, 594 and 688 µm/year, respectively. Therefore, it was confirmed that the Solar Salt cannot be used at high operating temperatures.

Liu et al. (2014) experimentally tested the corrosion of Hastelloy C22 immersed in two molten alkali chloride salts. The isothermal corrosion tests were conducted in air for 96 h. In KCl-NaCl (98.6–1.4 wt%), the corrosion rate of C22 at 700 °C is 405 µm/year. In KCl-NaCl (95.5–4.5 wt%), the corrosion rate at 650 °C is 310 µm/year. NiO, Cr<sub>2</sub>O<sub>3</sub> and Mo-containing compositions were the main corrosion products. Vignarooban et al. (2014) studied the corrosion rates of Hastelloy C276, C22 and N immersed in the NaCl-KCl-ZnCl<sub>2</sub> (74.5–23.9–68.6 wt%) eutectic mixture in air using the potentiodynamic method. Results indicate that C276 had the lowest corrosion rate of 40 µm/year and N had the highest corrosion rate of 150 µm/year at 500 °C.

Liu et al. (2017) studied the corrosion behavior of Ni-based alloys In625 and Hastelloy X (HX) in NaCl-CaCl<sub>2</sub>-MgCl<sub>2</sub> (53.43–31.61–14.95 mol.%) eutectic salt mixture in air atmosphere. SEM, EDS and XRD were used to characterize the corrosion products. The results show that the diffusion of Cr leads to poor Cr zone in the inner corrosion layer of In625 and HX. However, MgCr<sub>2</sub>O<sub>4</sub> attached to the surface formed a compact protective layer to resist further corrosion. The higher content of Fe in HX causes higher corrosion rate than In625. It was concluded that Ni and Mo in nickel-based alloys have higher stability during corrosion, and the addition of a certain amount

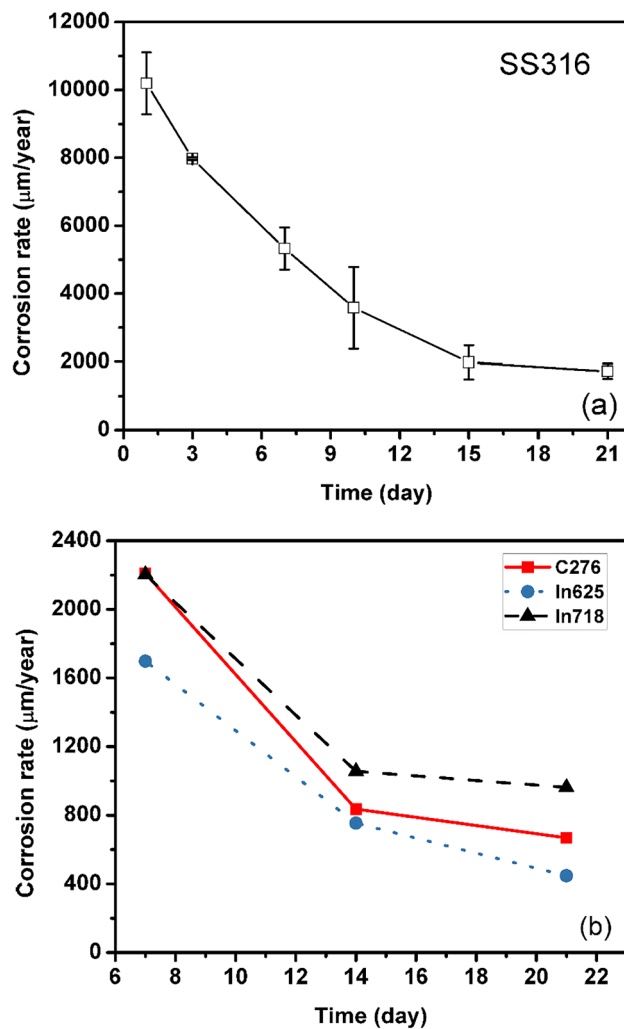


**Fig. 2.** Corrosion rates of the (a) SS316 and (b) C276, In625, In718 coupons immersed in the NaKZn chloride-salt at 700 °C for different days.

of Cr in the nickel-based alloys can enhance the corrosion resistance.

The SNL summarized corrosion of alloys immersed in chloride salts (Kruizenga, 2012). It was concluded that chloride salts showed preferential dissolution of alloying elements such as Cr. Chloride salts were susceptible to high corrosion rates in the presence of moisture and oxygen because stable and passivated oxide layers cannot be formed. Initial purity of salts was assumed to be responsible for the reported conflicting results in different studies. Refractory alloying elements are thought to improve the corrosion resistance in chloride salts due to the formation of stable spinel layer which prevents the diffusion of Cr from the base alloy to the salt mixture.

Carbonate-salts have been thoroughly investigated under the Molten Carbonate Fuel Cell (MCFC) operating conditions. However, the MCFC conditions are not applicable for CSP. In contrast, studies of carbonate-salts under high temperature and atmospheric conditions are very limited in the literature. An important parameter to understand the behavior of carbonate-salts is the basicity of the melt mixture. Olivares et al. (2012) pointed out that it was a significant issue to find alloys compatible with molten carbonates at temperatures higher than 400 °C. An early study of Coyle et al. (1986) showed that several commercial alloys including HX, Cabot 214, Haynes 188, Haynes 556, In750, Ni600 and Ni800 had corrosion rates of several millimeters per year in carbonate salts at 900 °C, which is completely unacceptable for CSP applications. Detailed studies have to be carried out to specifically quantify corrosion rates of alloys in carbonate salts at high temperatures.

Fluoride salt is particularly corrosive to metal alloys. Metals usually resist corrosion by forming oxidation films of Cr. However, the passivated oxide films are chemically unstable in molten fluoride salts. Therefore, corrosion of alloys is due to the thermodynamically driven dissolution of alloying elements into the fluoride salts (Olson, 2009). In Fe-Ni-Cr based alloys, Cr is the primary element that is most prone to dissolution particularly in the temperature range of 650–1200 °C (Olson et al., 2009). Liu et al. (2013) studied the corrosion behavior of Ni-based alloys In600, HX and C276 immersed in the molten LiF-NaF-KF (29.29–11.70–59.01 wt%) eutectic mixture. The experiments were conducted at 750 °C for 320 h in air atmosphere. The corrosion depth is 700, 300 and 100 μm for In600, HX and C276, respectively. The corresponding corrosion rates were not reported. It was suggested the high

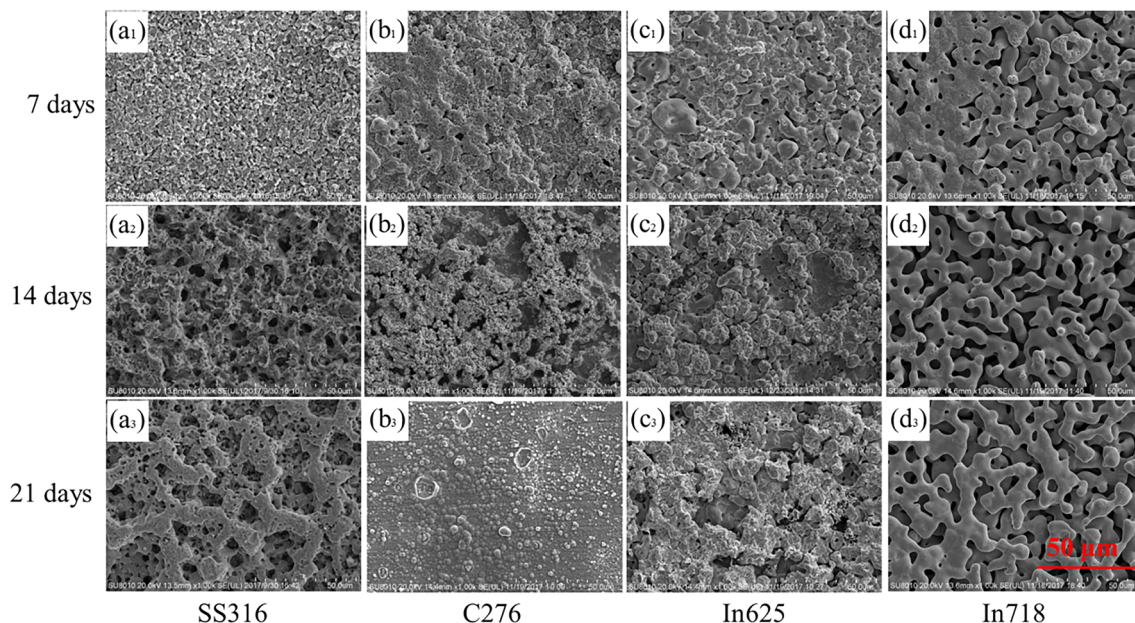


**Fig. 3.** Surface morphology development type A of the (a) SS316, (b) C276, (c) In625 and (d) In718 coupons in NaKZn chloride-salt for (1) 7 days, (2) 14 days and (3) 21 days.

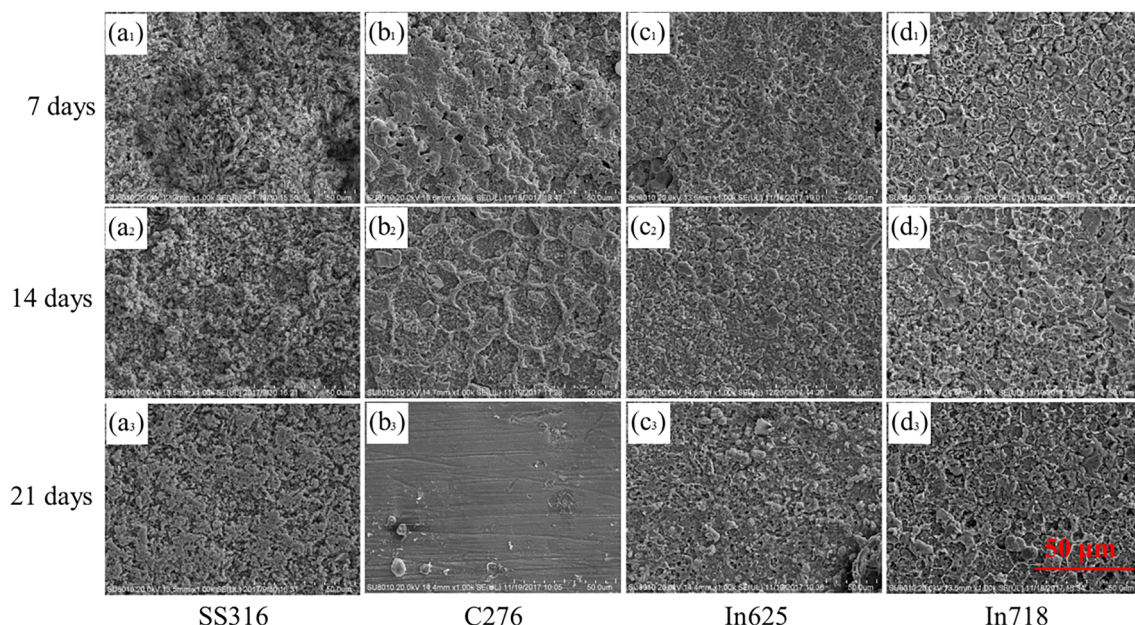


**Fig. 4.** Surface morphology development type B of the (a) SS316, (b) C276, (c) In625 and (d) In718 coupons in NaKZn chloride-salt for (1) 7 days, (2) 14 days and (3) 21 days.

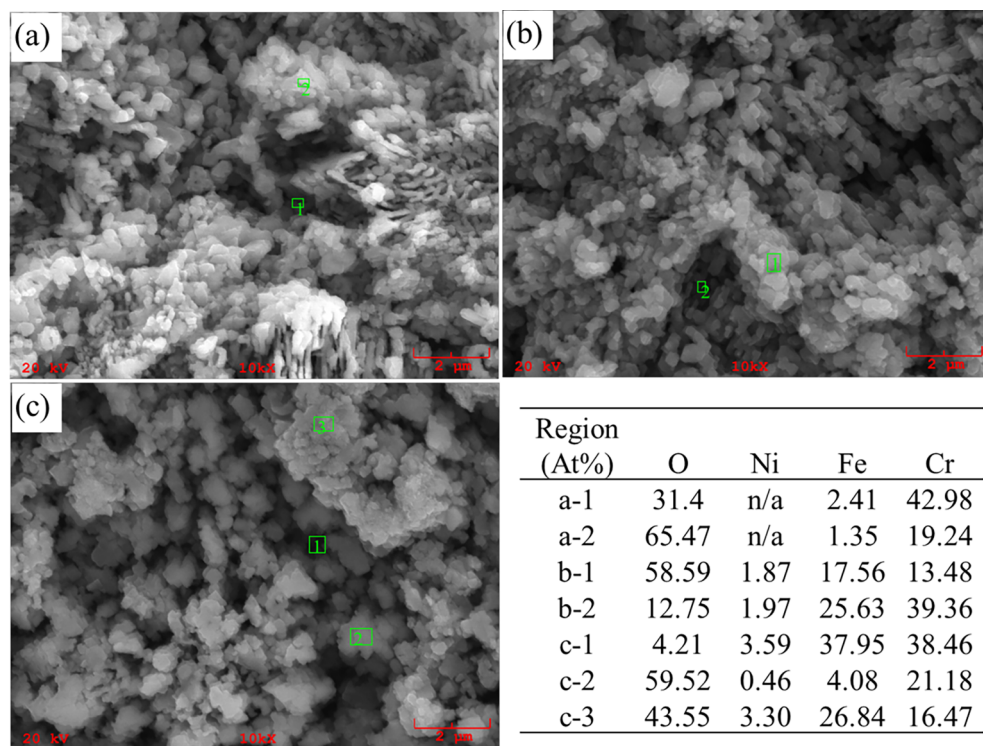


**Fig. 5.** EDS analysis of the SS316 coupon in the NaKZn chloride-salt immersed for (a) 7 days, (b) 14 days and (c) 21 days.

Mo content (15.49 wt%) and low Cr content (15.25 wt%) contribute to the highest corrosion resistance of C276.

In the present study, three HTF candidates with good thermo-physical properties including NaCl-KCl-ZnCl<sub>2</sub>, Li<sub>2</sub>CO<sub>3</sub>-Na<sub>2</sub>CO<sub>3</sub>-K<sub>2</sub>CO<sub>3</sub>, and LiF-Na<sub>2</sub>CO<sub>3</sub>-K<sub>2</sub>CO<sub>3</sub> mixtures were thoroughly investigated in regarding with their corrosion properties to SS316, C276, In625 and In718. Experiments were conducted under air atmosphere at 700 °C in

the chloride-salt mixture, the carbonate-salt mixture, and the fluoride-carbonate-salt mixture. [Section 2](#) presented the experimental method and procedures in details. SEM, EDS and XRD were employed to characterize the tested alloy specimens. In [Section 3](#), corrosion rates of different alloys in each molten-salt mixture were compared and the corrosion products were analyzed. Feasibility of each molten-salt mixture to be used as the HTF was evaluated.

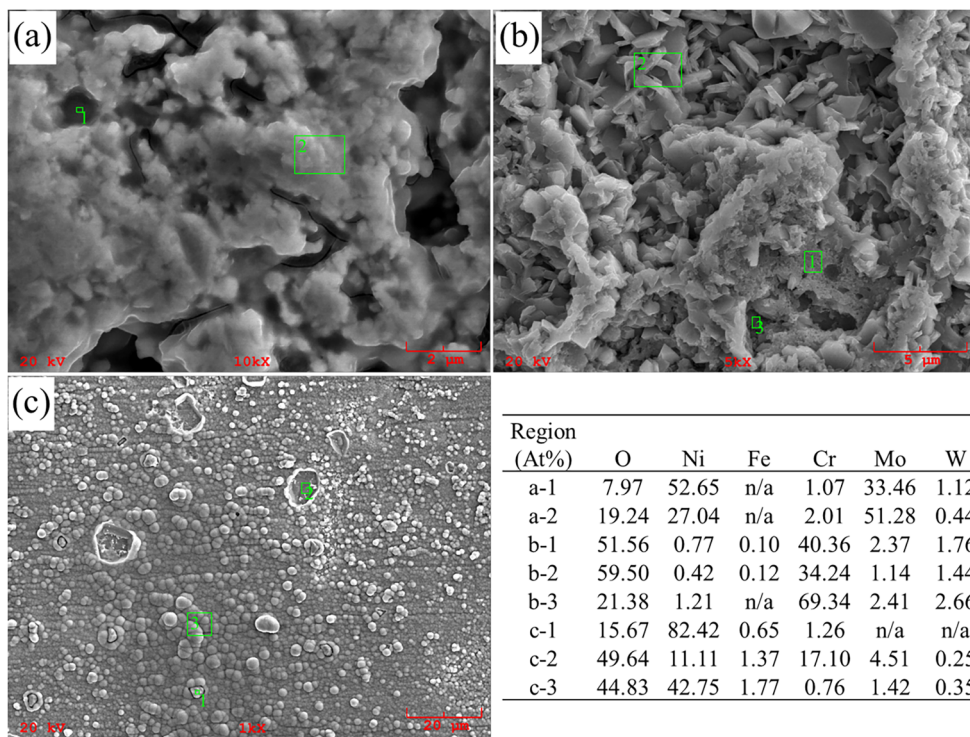


Fig. 6. EDS analysis of the C276 coupon in the NaKZn chloride-salt immersed for (a) 7 days, (b) 14 days and (c) 21 days.

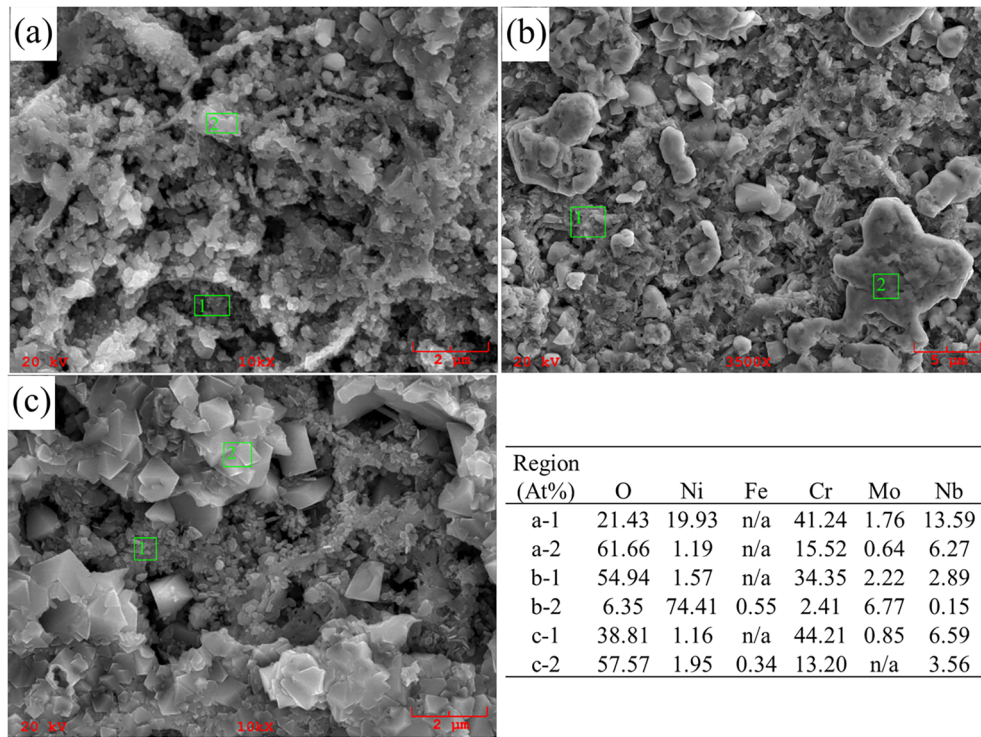


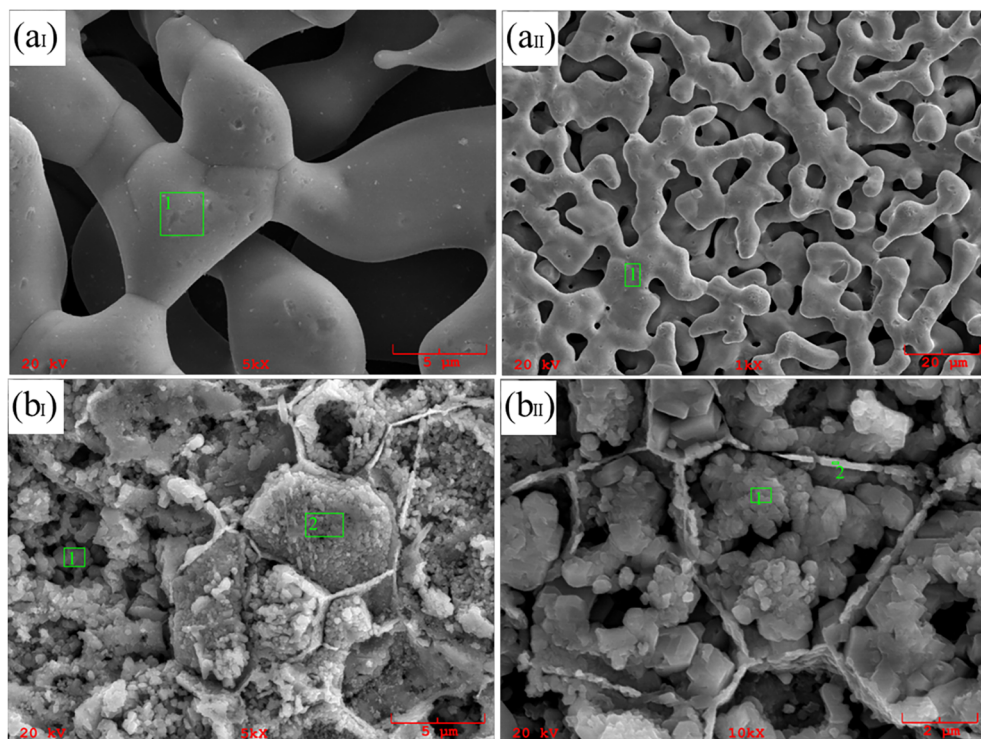
Fig. 7. EDS analysis of the In625 coupon immersed in the NaKZn chloride-salt for (a) 7 days, (b) 14 days and (c) 21 days.

## 2. Experimental

### 2.1. Material properties

Composition mass fractions of the three tested eutectic salt mixtures are NaCl-KCl-ZnCl<sub>2</sub> (8.1–31.3–60.6 wt%), Li<sub>2</sub>CO<sub>3</sub>-Na<sub>2</sub>CO<sub>3</sub>-K<sub>2</sub>CO<sub>3</sub> (32.1–33.4–34.5 wt%) and LiF-Na<sub>2</sub>CO<sub>3</sub>-K<sub>2</sub>CO<sub>3</sub> (17.7–28.1–54.2 wt%).

**Table 1** shows important thermophysical properties of the three salt mixtures. The NaKZn chloride-salt has the lowest melting point of 229 °C, which reduces the solidification risk in operation while the ambient temperature is relatively low at night (Li et al., 2016). The thermally stable temperatures of the NaKZn chloride-salt and the LiF-NaK carbonate-salt are both up to 800 °C (Li et al., 2016; Wang et al., 2015). The LiNaK carbonate-salt has a relatively lower thermally stable



Region (At%)	O	Ni	Fe	Cr	Mo	Nb
a <sub>I</sub> -1	6.87	78.44	n/a	n/a	7.17	0.32
a <sub>II</sub> -1	4.36	76.89	10.17	0.61	3.34	n/a
b <sub>I</sub> -1	58.52	0.63	n/a	13.69	0.54	19.21
b <sub>I</sub> -2	59.92	0.63	n/a	11.49	0.23	17.91
b <sub>II</sub> -1	65.90	0.53	n/a	9.05	0.65	17.21
b <sub>II</sub> -2	58.81	0.34	n/a	5.63	n/a	10.50

**Fig. 8.** EDS analysis of the (a) A type and (b) B type morphology development for the In718 coupon immersed in the NaKZn chloride-salt after (I) 14 days and (II) 21 days.

temperature than the other two salt mixtures. The thermal conductivity of the LiF-NaK carbonate-salt is 2–3 times higher than that of the other two salt mixtures, which suggests that it has better heat transfer performance as a HTF. The heat capacities of the LiNaK carbonate-salt and the LiF-NaK carbonate-salt are about two folds of that of the NaKZn chloride-salt.

The four tested high temperature alloys are SS316, C276, In625 and In718. Except for SS316, the others are all nickel based alloys. Table 2 lists the detailed compositions of each tested alloy. SS316 has the highest Fe content of 62–69 wt% and the lowest Ni content of 9.5–13 wt %. In718 has relatively higher Fe content of 11–22 wt% than C276 and In625. In625 and In718 have higher Cr content than the other two alloys. Mo, W, Ta, Nb, V and Ti are all refractory elements, which are expected to improve the corrosion resistance of alloys in molten salts (Kruizenga, 2012). C276 has obviously higher Mo and W contents than the others. In625 and In718 have slight higher content of Nb than SS316 and C276. However, the contents of Ta, V and Ti in the tested alloys are only in trace amounts if there is any.

## 2.2. Material preparation, cleaning, and characterization

Analytical grade (AR) chemicals were used to prepare the eutectic salt mixtures. The chemical suppliers and the purity of raw salts are

listed in Table 3. ZnCl<sub>2</sub> was separately stored in vacuum because of its high hydroscopic nature. The other salts were stored in desiccant chambers. All the salts were handled in a glove box under ultra-high purity (UHP) argon gas (99.999%) atmosphere. For each eutectic mixture, the pre-weighed salt compositions were mechanically mixed homogeneously before loading them into the quartz tube or corundum crucible.

The alloy specimen was cut into rectangular pieces (34 mm × 10 mm × 1 mm) before testing. The American Society for Testing Materials (ASTM) Standard G1-03 (2011) was applied to prepare and clean the alloy coupon. The fresh specimen was first rinsed by DI water and then polished by 600 and 1200 grit sandpapers in sequence. After that, DI water and acetone were used to rinse the coupon again. After drying in air, the initial mass of the prepared fresh specimen was weighed by an analytical balance with an accuracy of 0.1 mg.

After immersion tests, the alloy coupon was first sonicated in DI water for 15 min, and followed by a 15 min sonication in 5.55 wt% HCl solution. The cleaning process was repeated twice and then the coupon was sonicated in DI water for 15 min again before rinsing by acetone and drying in air. The dry coupon was weighed in an analytical balance and the mass was recorded. In order to make sure the sonication in 5.55 wt% HCl solution does not damage the alloy coupon, the HCl

**Table 4**

Main corrosion products of alloys immersed in different salts detected by XRD.

	7 days	14 days	21 days
<i>In NaKZn chloride-salt:</i>			
SS316	Fe <sub>9.7</sub> Mo <sub>0.3</sub> (2.3) NiFe <sub>2</sub> O <sub>4</sub> (17.4) ZnCr <sub>2</sub> O <sub>4</sub> (12.2) NiCrFeO <sub>4</sub> (39.1) NiCr <sub>2</sub> O <sub>4</sub> (29.0) MoNi <sub>4</sub> (13.5) Cr <sub>7</sub> Ni <sub>3</sub> (4.3) Mo <sub>1.24</sub> Ni <sub>0.76</sub> (53.4) FeNi (25.0) Fe <sub>3</sub> O <sub>4</sub> (3.7)	Fe <sub>9.7</sub> Mo <sub>0.3</sub> (4.3) <sup>a</sup> NiFe <sub>2</sub> O <sub>4</sub> (21.5) ZnCr <sub>2</sub> O <sub>4</sub> (10.6) NiCrFeO <sub>4</sub> (37.3) NiCr <sub>2</sub> O <sub>4</sub> (26.3) MoNi <sub>4</sub> (7.4) (Cr <sub>0.7</sub> V <sub>0.3</sub> ) <sub>2</sub> O <sub>3</sub> (10.2) Mo <sub>1.24</sub> Ni <sub>0.76</sub> (27.1) FeNi (32.7) Fe <sub>3</sub> O <sub>4</sub> (11.7) FeCr <sub>2</sub> O <sub>4</sub> (2.5) ZnCr <sub>2</sub> O <sub>4</sub> (3.1) Fe <sub>21.333</sub> O <sub>32</sub> (5.3)	Fe <sub>9.7</sub> Mo <sub>0.3</sub> (4.0) NiFe <sub>2</sub> O <sub>4</sub> (17.1) ZnCr <sub>2</sub> O <sub>4</sub> (7.6) NiCrFeO <sub>4</sub> (45.6) NiCr <sub>2</sub> O <sub>4</sub> (25.6) NiFe <sub>2</sub> O <sub>4</sub> (13.4) (Cr <sub>0.7</sub> V <sub>0.3</sub> ) <sub>2</sub> O <sub>3</sub> (4.2) (Cr <sub>1.9</sub> V <sub>0.09</sub> Fe <sub>0.01</sub> ) <sub>3</sub> (8.1) MoNi (19.6) MoNi <sub>4</sub> (3.8) FeNi (18.0) FeCr <sub>2</sub> O <sub>4</sub> (10.1) ZnCr <sub>2</sub> O <sub>4</sub> (8.0) Fe <sub>21.333</sub> O <sub>32</sub> (14.8) Ni <sub>2.9</sub> Cr <sub>0.7</sub> Fe <sub>0.36</sub> (57.9) CrNbO <sub>4</sub> (3.5) MoNi (12.1) FeNi <sub>3</sub> (9.2) Cr <sub>2</sub> O <sub>3</sub> (2.6) CrMoO <sub>3</sub> (2.6) NiCrFeO <sub>4</sub> (3.4) Zn <sub>0.5</sub> Ni <sub>0.5</sub> FeCrO <sub>4</sub> (4.9) Ti <sub>0.2</sub> Cr <sub>0.4</sub> Nb <sub>0.4</sub> O <sub>2</sub> (3.8) Ni <sub>2.9</sub> Cr <sub>0.7</sub> Fe <sub>0.36</sub> (86.6) Ti <sub>0.4</sub> Fe <sub>0.3</sub> Nb <sub>0.3</sub> O <sub>2</sub> (2.8) Cr <sub>1.776</sub> Mo <sub>0.112</sub> O <sub>3</sub> (1.6) Cr <sub>2</sub> O <sub>3</sub> (0.9) FeNi <sub>3</sub> (8.1)
In625	Ni <sub>2.9</sub> Cr <sub>0.7</sub> Fe <sub>0.36</sub> (81.5) CrNbO <sub>4</sub> (0.2) MoNi (17.5) Fe <sub>3</sub> Ni <sub>2</sub> (0.8)	Ni <sub>2.9</sub> Cr <sub>0.7</sub> Fe <sub>0.36</sub> (71.4) CrNbO <sub>4</sub> (1.3) MoNi (12.1) FeNi <sub>3</sub> (11.4) NiCrFeO <sub>4</sub> (1.1) Zn <sub>0.5</sub> Ni <sub>0.5</sub> FeCrO <sub>4</sub> (1.9) Ti <sub>0.2</sub> Cr <sub>0.4</sub> Nb <sub>0.4</sub> O <sub>2</sub> (0.8)	Ni <sub>2.9</sub> Cr <sub>0.7</sub> Fe <sub>0.36</sub> (57.9) CrNbO <sub>4</sub> (3.5) MoNi (12.1) FeNi <sub>3</sub> (9.2) Cr <sub>2</sub> O <sub>3</sub> (2.6) CrMoO <sub>3</sub> (2.6) NiCrFeO <sub>4</sub> (3.4) Zn <sub>0.5</sub> Ni <sub>0.5</sub> FeCrO <sub>4</sub> (4.9) Ti <sub>0.2</sub> Cr <sub>0.4</sub> Nb <sub>0.4</sub> O <sub>2</sub> (3.8) Ni <sub>2.9</sub> Cr <sub>0.7</sub> Fe <sub>0.36</sub> (86.6) Ti <sub>0.4</sub> Fe <sub>0.3</sub> Nb <sub>0.3</sub> O <sub>2</sub> (2.8) Cr <sub>1.776</sub> Mo <sub>0.112</sub> O <sub>3</sub> (1.6) Cr <sub>2</sub> O <sub>3</sub> (0.9) FeNi <sub>3</sub> (8.1)
In718	Ni <sub>2.9</sub> Cr <sub>0.7</sub> Fe <sub>0.36</sub> (82.6) Ti <sub>0.4</sub> Fe <sub>0.3</sub> Nb <sub>0.3</sub> O <sub>2</sub> (9.6) Cr <sub>2</sub> O <sub>3</sub> (0.8) FeNi <sub>3</sub> (7.0)	Ni <sub>2.9</sub> Cr <sub>0.7</sub> Fe <sub>0.36</sub> (86.2) Ti <sub>0.4</sub> Fe <sub>0.3</sub> Nb <sub>0.3</sub> O <sub>2</sub> (0.7) FeNi <sub>3</sub> (13.1)	Ni <sub>2.9</sub> Cr <sub>0.7</sub> Fe <sub>0.36</sub> (86.6) Ti <sub>0.4</sub> Fe <sub>0.3</sub> Nb <sub>0.3</sub> O <sub>2</sub> (2.8) Cr <sub>1.776</sub> Mo <sub>0.112</sub> O <sub>3</sub> (1.6) Cr <sub>2</sub> O <sub>3</sub> (0.9) FeNi <sub>3</sub> (8.1)
<i>In LiNaK carbonate-salt:</i>			
SS316	n/a	n/a	(NiO) <sub>0.75</sub> (MnO) <sub>0.25</sub> (35) Li <sub>0.28</sub> Fe <sub>21.34</sub> O <sub>32</sub> (65)
C276	n/a	n/a	Li <sub>0.79</sub> Ni <sub>1.21</sub> O <sub>2</sub> (6.4) LiCrO <sub>2</sub> /Li <sub>2</sub> O-Cr <sub>2</sub> O <sub>3</sub> (21.9) Ni(71.7)
In625	FeNi <sub>3</sub> (10.1) LiCrO <sub>2</sub> (17.1) FeNi(21.6) Ni <sub>2.9</sub> Cr <sub>0.7</sub> Fe <sub>0.36</sub> (51.1)	FeNi <sub>3</sub> (4.7) Ni <sub>2.9</sub> Cr <sub>0.7</sub> Fe <sub>0.36</sub> (19.8) Li <sub>0.68</sub> Ni <sub>1.32</sub> O <sub>2</sub> (8.6) Li <sub>0.79</sub> Ni <sub>1.21</sub> O <sub>2</sub> (10.6) Li <sub>0.92</sub> Ni <sub>1.08</sub> O <sub>2</sub> (11.8) Ni(44.5)	Li <sub>0.68</sub> Ni <sub>1.32</sub> O <sub>2</sub> (6.9) Li <sub>0.79</sub> Ni <sub>1.21</sub> O <sub>2</sub> (9.0) Li <sub>0.92</sub> Ni <sub>1.08</sub> O <sub>2</sub> (8.2) Ni(76.0)
In718	n/a	n/a	LiCrO <sub>2</sub> / Li <sub>2</sub> O-Cr <sub>2</sub> O <sub>3</sub> (40.2) FeNi <sub>3</sub> (59.8)
<i>In LiF-NaK carbonate-salt:</i>			
SS316	n/a	(MgO) <sub>0.593</sub> (FeO) <sub>0.407</sub> (1.8) Li <sub>0.3</sub> CoFe <sub>2</sub> O <sub>4</sub> (43.3) LiCrO <sub>2</sub> /Li <sub>2</sub> O-Cr <sub>2</sub> O <sub>3</sub> (54.9)	(MgO) <sub>0.91</sub> (FeO) <sub>0.09</sub> (77.3) LiCrO <sub>2</sub> /Li <sub>2</sub> O-Cr <sub>2</sub> O <sub>3</sub> (21.1) Li(Mn <sub>0.9167</sub> Cr <sub>0.0833</sub> ) <sub>2</sub> O <sub>4</sub> (1.6)
C276	Li <sub>0.65</sub> Ni <sub>1.08</sub> O <sub>2</sub> (1.6) Li <sub>0.68</sub> Ni <sub>1.32</sub> O <sub>2</sub> (3.6) LiCrO <sub>2</sub> /Li <sub>2</sub> O-Cr <sub>2</sub> O <sub>3</sub> (6.2) Ni(88.6)	Li <sub>0.65</sub> Ni <sub>1.08</sub> O <sub>2</sub> (1.7) Li <sub>0.68</sub> Ni <sub>1.32</sub> O <sub>2</sub> (2.4) LiCrO <sub>2</sub> /Li <sub>2</sub> O-Cr <sub>2</sub> O <sub>3</sub> (8.9) Ni(87.0)	Li <sub>0.65</sub> Ni <sub>1.08</sub> O <sub>2</sub> (2.6) Li <sub>0.68</sub> Ni <sub>1.32</sub> O <sub>2</sub> (2.7) LiCrO <sub>2</sub> /Li <sub>2</sub> O-Cr <sub>2</sub> O <sub>3</sub> (13.1) Ni(81.7)
In625	n/a	n/a	Li <sub>0.65</sub> Ni <sub>1.08</sub> O <sub>2</sub> (3.9) Li <sub>0.2</sub> V <sub>1.16</sub> O <sub>2</sub> (5.3) LiCrO <sub>2</sub> (8.8) LiV <sub>2</sub> O <sub>4</sub> (9.8) Ni(13.1) FeNi(59.0)
In718	n/a	Li <sub>0.65</sub> Ni <sub>1.08</sub> O <sub>2</sub> (5.5) LiCrO <sub>2</sub> /Li <sub>2</sub> O-Cr <sub>2</sub> O <sub>3</sub> (39.0) FeNi <sub>3</sub> (55.5)	n/a

Note: The number after each composition denotes the mass fraction.

<sup>a</sup> The results are obtained after 15 days tests instead of 14 days.

pickling was repeated 10 times for two fresh specimen of C276 and In625. No mass change was observed and the standard deviations of the specimen mass weighed after each pickling were both  $10^{-5}$ , which confirms that the pickling process does not affect the alloy coupon but

only removes products formed due to corrosion.

SEM (Hitachi SU8010) was used to characterize the morphology of the corroded surfaces of the tested alloy coupons. Chemical compositions in the surfaces of the tested coupons were analyzed by EDS (IXRF

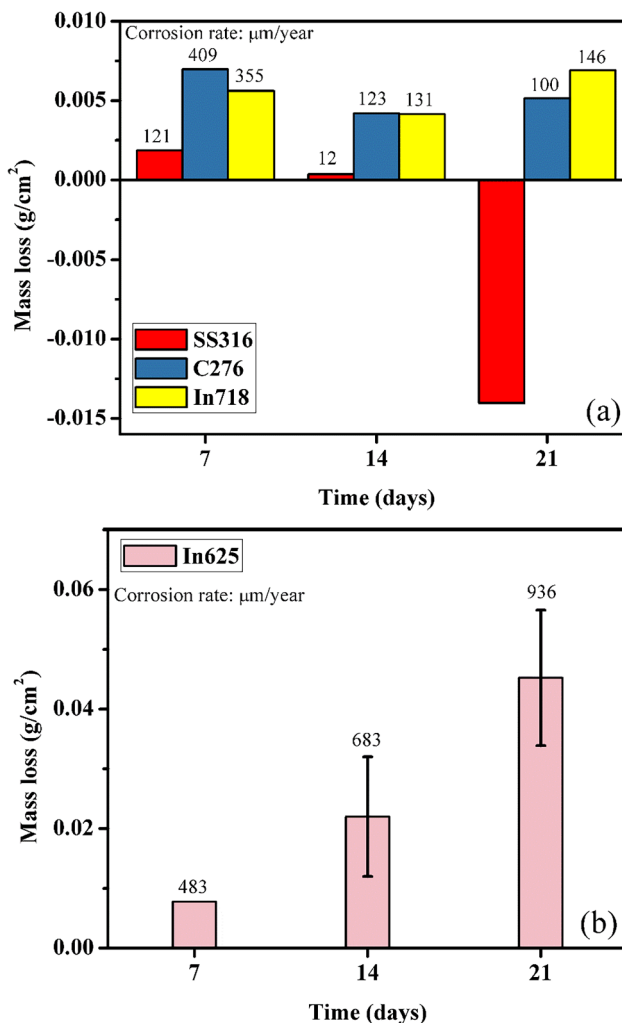


**Fig. 9.** Mass loss of the (a) SS316, C276, In718 and (b) In625 coupons immersed in the LiNaK carbonate-salt at 700 °C for 7, 14 and 21 days.

model 550i). XRD (BRUKER-AXS D8 Advance) was used to characterize the crystallographic structures of the corrosion products on the surfaces of the alloy coupons.

### 2.3. Experimental procedure

The prepared alloy coupon was immersed in the solid salt mixture. The NaKZn chloride-salt was contained in a quartz tube. The LiNaK carbonate-salt or the LiF-NaK carbonate-salt was put in a corundum crucible because the carbonate salts can react with quartz at high temperatures. The quartz tube or corundum crucible were then put in a

furnace as shown in Fig. 1. The cap on top of the quartz tube or corundum crucible was used to maintain enough salt mixtures in the liquid phase containing the alloy coupon after long time immersion tests. Otherwise all molten-salt mixtures would turn to gaseous phase within two days because the evaporation rates of salts at temperature close to the boiling point are very high. The caps are not tightly closed and air is able to access into the quartz tube or corundum crucible through the clearance between the cap and container. The heating rate of the furnace was set at 3 °C/min. In order to reduce the temperature gradient inside the salt mixture, the heating process held for 30 min with every 100 °C temperature increment. The isothermal corrosion tests were all conducted at 700 °C for the three salt mixtures. Various corrosion time including 7, 14 and 21 days were tested for each alloy in different salt mixtures. After the corrosion test, the furnace was cooled down at the rate of 2 °C/min to the ambient temperature. Then the alloy coupons were taken out for cleaning by dissolving the salt mixture in DI water at the ambient temperature.

Eq. (1) was used to calculate the corrosion rate based on the mass loss of the alloy coupon after immersion tests (Dorcheh et al., 2016),

$$CR = 365 \times 10^4 [(m_i - m_f)/\rho AT] \quad (1)$$

where CR is the corrosion rate, µm/year;  $m_f$  is the mass of the alloy coupon after immersion test, g;  $m_i$  is the mass of the fresh alloy coupon, g;  $\rho$  is the density of the alloy coupon, g/cm<sup>3</sup>; A is the immersed area of the alloy coupon, cm<sup>2</sup>; and T is the immersion test time, day.

## 3. Results and discussion

### 3.1. Corrosion of alloys in the chloride-salt mixture

Fig. 2 shows the corrosion rates of the SS316, C276, In625 and In718 coupons immersed in the NaKZn chloride-salt at 700 °C for different days. It can be seen that all alloy coupons were corroded severely under air atmosphere since the water vapor and oxygen in air have significant effects on corrosion. As the Fe element in the alloys would be preferential oxidization and chlorination, SS316 shows worse corrosion resistance than the other three Ni-based alloys. According to Fig. 2(a), the corrosion rate decreases rapidly in the beginning and then tends to become stable after 15 days immersion, which is in agreement with the typical corrosion behavior of alloys immersed in molten salts. This behavior suggests that the corrosion product is controlled by solid state diffusion growth process and the dissolution rate of the corrosion product in the molten chloride-salt is limited. After immersed in the chloride-salt mixture for 21 days, the converged corrosion rates are around 1700, 668, 447 and 962 µm/year for SS316, C276, In625 and In718, respectively.

SEM graphs of the four alloy coupons immersed in the NaKZn chloride-salt for 7, 14 and 21 days indicate that two types of surface morphology exist in different regions of the alloy surfaces, which are labeled as A type and B type in the present study. Fig. 3 shows the A type morphology development with large size pores. Moreover, the

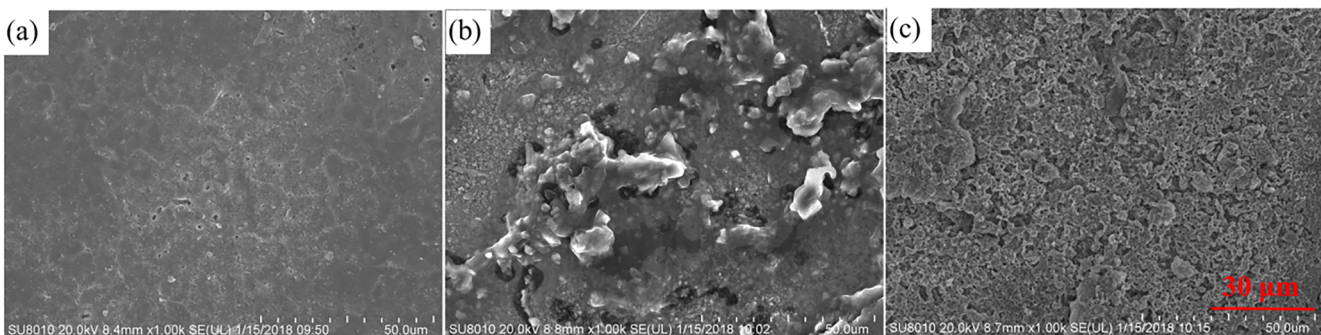


**Fig. 10.** SEM images of the (a) SS316, (b) C276 and (c) In718 coupons immersed in the LiNaK carbonate-salt at 700 °C for 21 days.

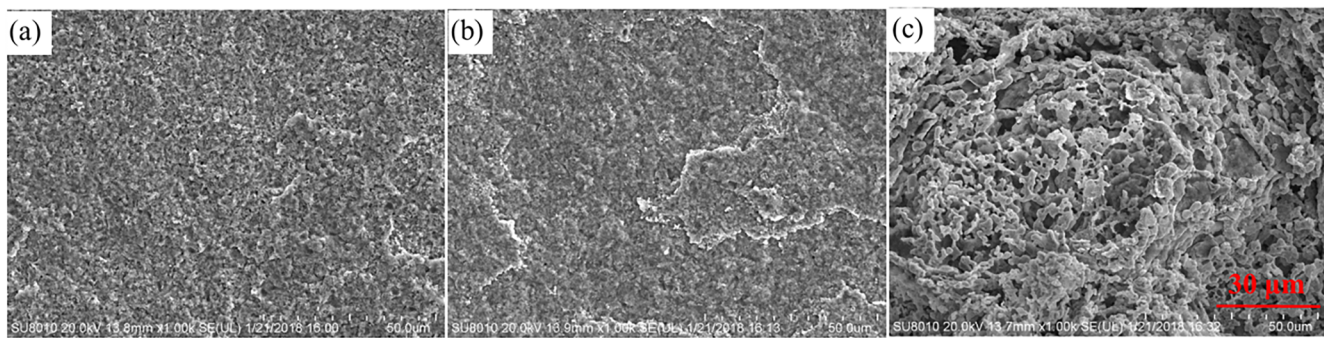


Fig. 11. SEM images of the In625 coupon immersed in the LiNaK carbonate-salt for (a) 7 days, (b) 14 days and (c) 21 days.

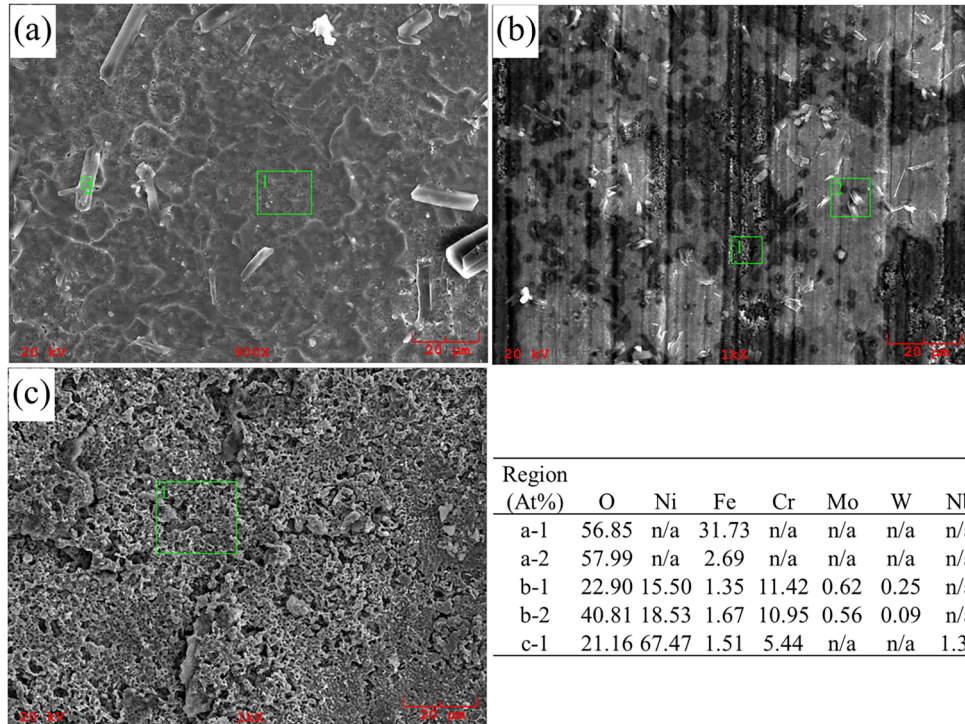


Fig. 12. EDS analysis of the (a) SS316, (b) C276 and (c) In718 coupons immersed in the LiNaK carbonate-salt at 700 °C for 21 days.

pore sizes increase and the surfaces become more uneven as the immersion time increases. The pore size on the SS316 and In718 surfaces is larger than that of C276 and In625. After 21 days immersion, multi-layer structure is observed on the surfaces of SS316, In625 and In718, while C276 exhibits a relative uniform surface with bubble structure. Cracks on the surface of In625 also become more intensive with the immersion time increases.

Fig. 4 shows the B type morphology development. Pores are much smaller than those in the A type morphology and the surfaces are less uneven. After 21 days immersion, small and dense particles were formed in the superficial layer, as well as a compact layer formed beneath the particles on the surfaces of SS316, In625 and In718. However, C276 shows a uniform surface without visible pores after 21 days immersion just like the superficial layer is peeled off. Cracks on the surface of In718 become denser as the immersion time increases from 7 to 21 days.

Figs. 5–8 show the EDS analysis of SS316, C276, In625 and In718 test coupons immersed in the NaKZn chloride-salt for different days. It can be seen from Fig. 5 that the Cr content in the outer layer is much lower than that in the inner layer after 7, 14 and 21 days immersion, which suggests that the surface protective Cr oxide layer can be destroyed by the molten-salt mixture. The corrosion for SS316 was mostly

caused by the dissolution of Cr element into the salt. Moreover, significant dissolution of Fe element is also observed in Fig. 5.

Fig. 6 shows the corrosion products of C276 are mainly (Ni and Mo)-rich compositions after 7 days immersion. Ni cannot form a stable protective layer because the content of Ni in the outer layer is lower than that in the inner layer. After 14 days immersion, Cr-rich corrosion products are also observed and the content of Cr in the outer layer is also lower than that in the inner layer. Fig. 6(c) indicates that only Ni content is rich on the surface after 21 days immersion. The Cr corrosion products could be dissolved in the molten-salt mixture during immersion test or be removed by ultrasonic washing before characterization.

The EDS results of In625 in Fig. 7 indicate that dissolution of both Ni and Cr occurred after 7 days immersion because their contents in the outer layer are less than those in the inner layer. After 14 days immersion, the Ni content increased while the Cr content decreased. The Cr corrosion products seem to dissolve preferentially in the molten chlorides. However, only Cr-rich products were detected after 21 days test and the Ni corrosion products could be destroyed by the salt mixture or cleaning procedure. In625 has the lowest corrosion rate compared to the other three alloys after 21 days immersion, which may be resulted from the formation of protective Cr oxide layer in the surface. For In718, Fig. 8 shows that Ni-rich oxides appeared in the outer layer

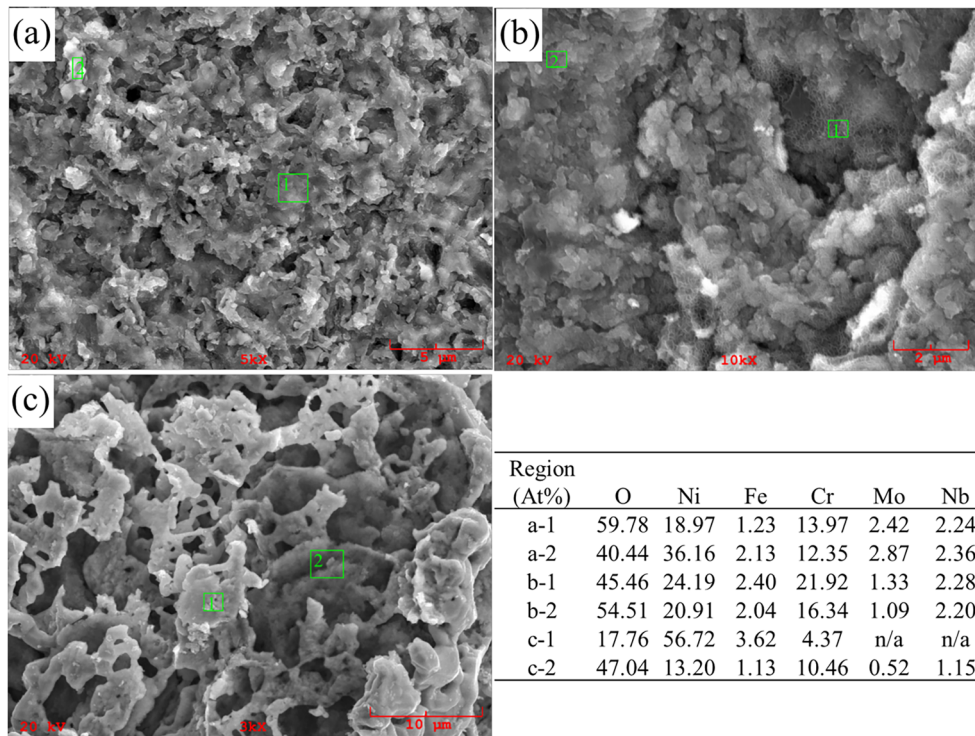


Fig. 13. EDS analysis of the In625 coupon immersed in the LiNaK carbonate-salt at 700 °C for (a) 7 days, (b) 14 days and (c) 21 days.

of A type morphology region after 14 and 21 days immersion. In contrast, Nb-rich products are the major corrosion products in the B type morphology region after 14 and 21 days immersion.

Table 4 lists the XRD analysis results of the SS316, C276, In625 and In718 coupons immersed in the NaKZn chloride-salt for 7, 14 and 21 days. It indicates that the corrosion product compositions on the surface of SS316 are almost independent of immersion time. The phases formed on the surface are primarily NiCrFeO<sub>4</sub>, NiCr<sub>2</sub>O<sub>4</sub>, NiFe<sub>2</sub>O<sub>4</sub> and ZnCr<sub>2</sub>O<sub>4</sub> with the spinel structure. However, these products did not prevent the diffusion of Cr from the base alloy to the salt mixture. None Cr<sub>2</sub>O<sub>3</sub> or Fe<sub>x</sub>O<sub>y</sub> is identified. Mo<sub>1.24</sub>Ni<sub>0.76</sub> and MoNi<sub>4</sub> are the major phases on the surface of C276 after 7 days test. (Cr<sub>0.7</sub>V<sub>0.3</sub>)<sub>2</sub>O<sub>3</sub> are detected after 14 days. NiFe<sub>2</sub>O<sub>4</sub>, FeCr<sub>2</sub>O<sub>4</sub> and ZnCr<sub>2</sub>O<sub>4</sub> with the spinel structure are the primary phases on the surface after 21 days immersion. Moreover, iron oxides (Fe<sub>3</sub>O<sub>4</sub> and Fe<sub>21.333</sub>O<sub>32</sub>) are identified from 7 to 21 days immersion. Ni<sub>2.9</sub>Cr<sub>0.7</sub>Fe<sub>0.36</sub> is the primary phase on the surface of In625, and its content decreases as the immersion time increases. After 21 days test, other phases containing Cr element such as CrNbO<sub>4</sub>, NiCrFeO<sub>4</sub>, Cr<sub>2</sub>O<sub>3</sub> and CrMoO<sub>3</sub> are also detected in the corrosion products. For In718, Ni<sub>2.9</sub>Cr<sub>0.7</sub>Fe<sub>0.36</sub> is the dominant phase in the corrosion products regardless of the immersion time. Ti<sub>0.4</sub>Fe<sub>0.3</sub>Nb<sub>0.3</sub>O<sub>2</sub> is also detected in the corrosion products.

### 3.2. Corrosion of alloys in the carbonate-salt mixture

Fig. 9 exhibits the mass loss of the SS316, C276, In625 and In718 coupons immersed in the LiNaK carbonate-salt mixture at 700 °C for different days. Fig. 9(a) shows that the SS316 coupon has mass gain instead of mass loss after 21 days immersion, which could be due to formation of layers difficult to dissolve in the molten salt mixture. The corrosion rate is relative low for C276 and In718, which is 100 and 146 μm/year after 21 days test, respectively. In contrast, the mass loss

of the In625 coupon increased with the immersion time as shown in Fig. 9(b), and the corresponding corrosion rate increased from 483 to 936 μm/year as the immersion time increased from 7 to 21 days.

Figs. 10 and 11 show the SEM images of the four alloy coupons immersed in the LiNaK carbonate-salt for different days. After 21 days immersion, the surface of SS316 is quite uniform without noticeable pores or cracks. Relatively large particles are observed on the surface of C276 after 21 days immersion. Small pores and multi-layer structure appear on the surface of In718 after 21 days immersion. Although the calculated corrosion rate is relatively low, the surface morphology of IN718 indicates that the corrosion is not controllable because of the pores. For In625, the surface became more uneven as the immersion time increased. Multi-layer structure and large pores are observed on the surface of In625 after 21 days immersion.

EDS analysis of the SS316, C276, In718 and In625 coupons after immersion are shown in Figs. 12 and 13, and the corresponding XRD results are tabulated in Table 4. Fe-rich composition is observed on the surface of SS316 after 21 days immersion, which is in the major phase of Li<sub>9.28</sub>Fe<sub>21.34</sub>O<sub>32</sub> according to the XRD results. Since the uniform and dense layer observed by SEM as shown in Fig. 10(a) is rich in Fe, the corrosion resistance of SS316 immersed in the carbonate-salt mixture is questionable. Fe oxide layer is usually not stable and has risk to completely peel off during operation. After 21 days immersion, (Ni and Cr)-rich compositions are detected on the surface of C276. Protective Cr oxide layer may be formed and contribute to the relative low corrosion rate of C276. XRD results indicate that the major phases on the surface of C276 are Ni and LiCrO<sub>2</sub>/Li<sub>2</sub>O-Cr<sub>2</sub>O<sub>3</sub>. FeNi<sub>3</sub> is the major phase detected by XRD on the surface corrosion products of In718. Since many small pores and multi-layer structure are observed by SEM, it can be deduced that no protective Ni oxide layer formed on the surface of In718.

For In625, the compositions of Ni and Cr were rich regardless of the

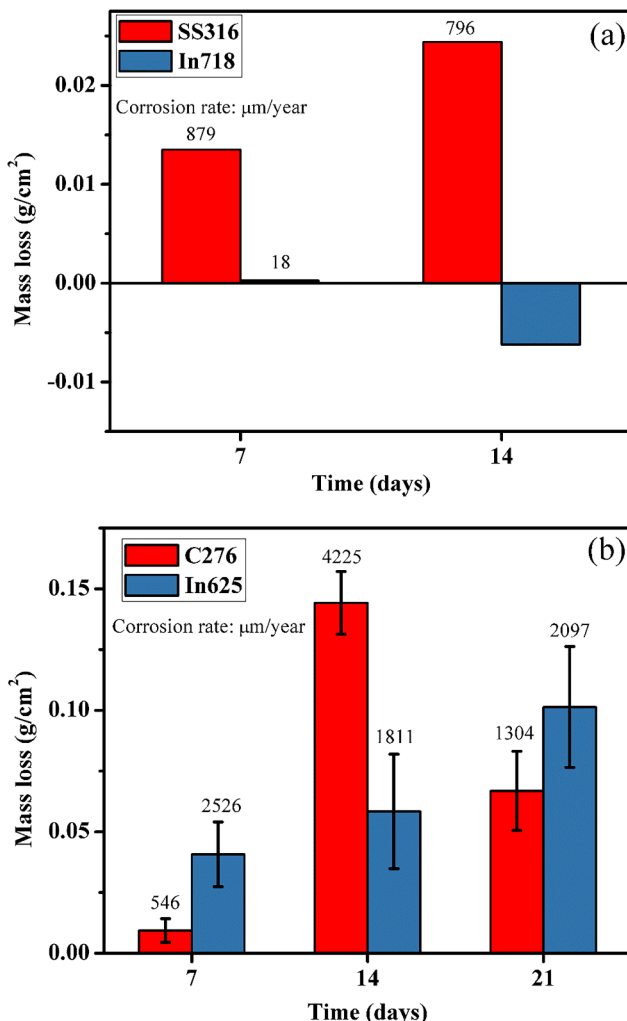


**Fig. 14.** Mass loss of the (a) SS316, In718 and (b) C276, In625 coupons immersed in the LiF-NaK carbonate-salt at 700 °C for 7 and 14 days.

immersion time. High content of Ni appeared after 14 and 21 days immersion as shown by the XRD results. The reaction between Li<sub>2</sub>CO<sub>3</sub> and In625 seems to contribute to the increasing corrosion rate with immersion time, because the rest major phases in the corrosion products after 21 days immersion are Li<sub>0.79</sub>Ni<sub>1.21</sub>O<sub>2</sub>, Li<sub>0.92</sub>Ni<sub>1.08</sub>O<sub>2</sub> and Li<sub>0.68</sub>Ni<sub>1.32</sub>O<sub>2</sub>.

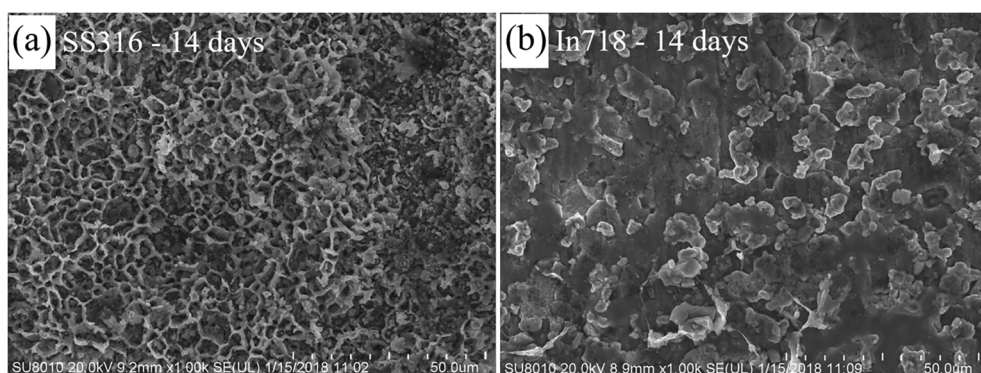


**Fig. 15.** SEM images of the (a) SS316 and (b) In718 coupons immersed in the LiF-NaK carbonate-salt at 700 °C for 14 days.

### 3.3. Corrosion of alloys in the fluoride-carbonate-salt mixture

Fig. 14 shows the mass loss of the SS316, C276, In625 and In718 coupons immersed in the LiF-NaK carbonate-salt mixture at 700 °C for different days. Fig. 14 (a) indicates that the SS316 coupon has severe corrosion after 14 days test, and the In718 coupon has mass gain instead of mass loss after 14 days immersion. According to the corresponding SEM images in Fig. 15, the surface of SS316 has multi-layer structure with large pores, while the surface of In718 has relative dense morphology without visible pores. The mass gain could be due to the formation of protective layers. The XRD results in Table 4 indicate that the corrosion products on the surface of In718 are main in the phases of LiCrO<sub>2</sub> and Li<sub>2</sub>O-Cr<sub>2</sub>O<sub>3</sub>. Both are protective layers which could prevent dissolution of alloying elements to the molten salts.

Fig. 14(b) demonstrates that both the C276 and In625 coupons have severe corrosion in the LiF-NaK carbonate-salt mixture. The corrosion rates of C76 and In625 after 21 days immersion test are 1304 and 2097 µm/year, respectively. According to the corresponding SEM images in Fig. 16, the surfaces of both alloys are uneven with significant multi-layer structure and small pores.

The EDS results in Figs. 17 and 18 indicate that the (Ni and Cr)-rich compositions are detected on the surfaces of both C276 and In625 immersed in the LiF-NaK carbonate-salt mixture. Table 4 demonstrates that the major phases are Ni and LiCrO<sub>2</sub>/Li<sub>2</sub>O-Cr<sub>2</sub>O<sub>3</sub> on the surface of C276 immersed in the LiF-NaK carbonate-salt mixture, which are the same as phases detected for C276 immersed in the LiNaK carbonate-salt mixture. However, the extreme high corrosion rate of C276 immersed in the LiF-NaK carbonate-salt mixture suggests that the layers of LiCrO<sub>2</sub> and Cr<sub>2</sub>O<sub>3</sub> are unstable because of the existence of LiF instead of LiCO<sub>3</sub>. For In625, the rest major phases in the corrosion products immersed in the LiF-NaK carbonate-salt mixture after 21 days immersion are LiCrO<sub>2</sub> and LiV<sub>2</sub>O<sub>4</sub>.

### 3.4. Discussion

The corrosion rates of four alloys in three eutectic salt mixtures at 700 °C for 21 days under air atmosphere are summarized in Table 5. It can be seen that none of tested alloy combines with NaKZn chloride-salt could meet the requirements for CSP commercial applications (corrosion rate < 10 µm/year, Ding et al., 2018) under air atmosphere. Therefore, the NaKZn chloride-salt is not applicable as a HTF if air cannot be evacuated.

In the LiNaK carbonate-salt mixture, C276 shows a relative low corrosion rate of 100 µm/year. Protective Cr oxide layer may be formed on its surface. Although In718 also has a relative low corrosion rate of 146 µm/year, it is not corrosion resistant to the LiNaK carbonate-salt mixture because SEM image of its surface indicates porous and multi-

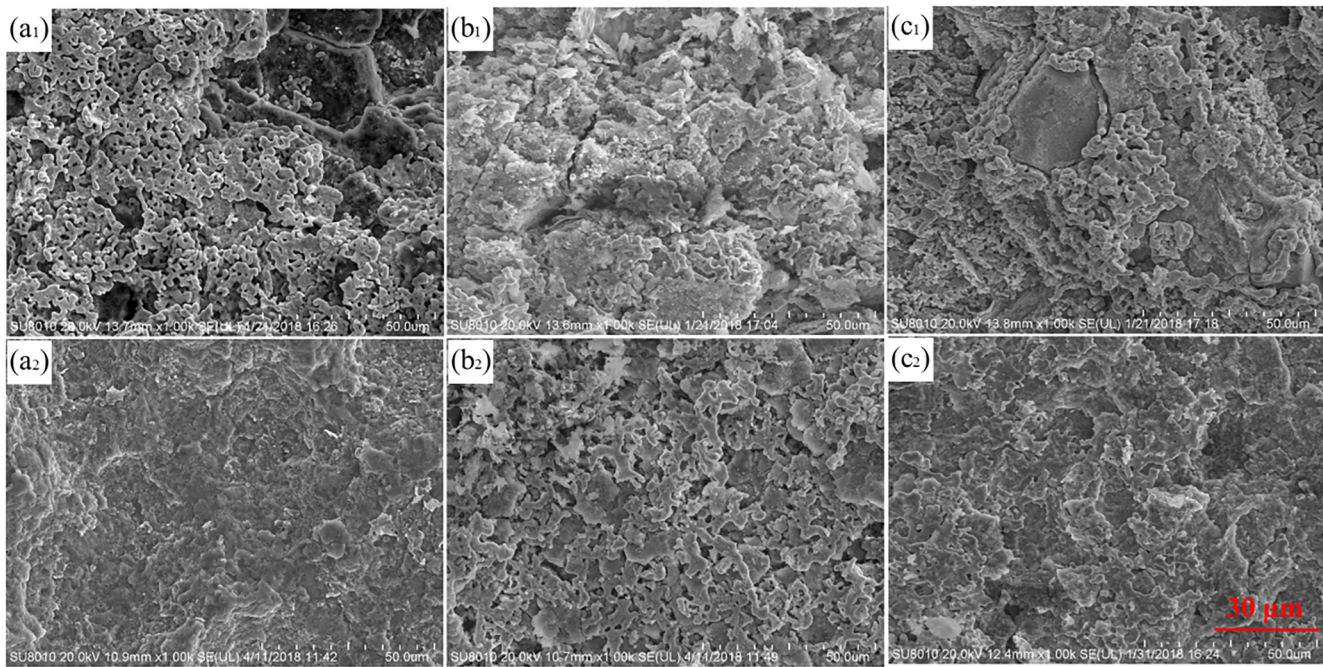


**Fig. 16.** SEM images of the (1) C276 and (2) In625 coupons immersed in the LiF-NaK carbonate-salt at 700 °C for (a) 7 days, (b) 14 days and (c) 21 days.

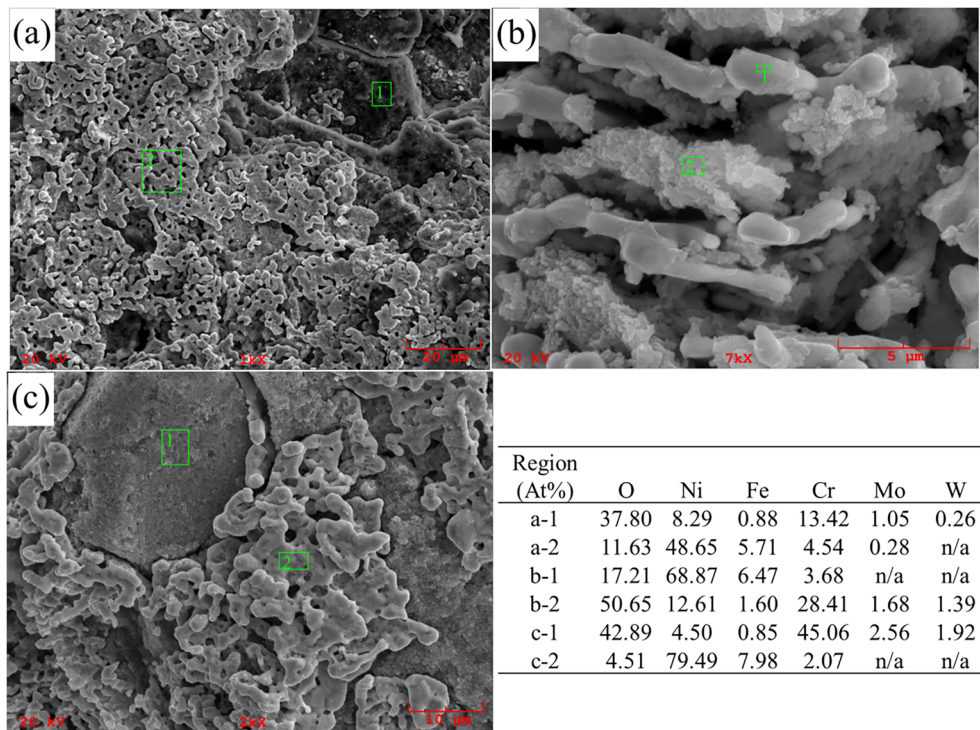


**Fig. 17.** EDS analysis of the C276 coupon immersed in the LiF-NaK carbonate-salt at 700 °C for (a) 7 days, (b) 14 days and (c) 21 days.

layer structure. As for the LiF-NaK carbonate-salt mixture, SS316, C276 and In625 all have extremely high corrosion rates.

The combinations of LiNaK carbonate-salt/SS316 and LiF-NaK carbonate-salt/In718 show mass gain instead of mass loss, which are suspected resulted from formation of protective compact layers on surface of the alloys. However, EDS analyses indicate that the surface layer of SS316 immersed in the LiNaK carbonate-salt is rich in Fe. Fe oxide layer is usually not stable and tends to completely peel off during operation. Protective layers of  $\text{LiCrO}_2$  and  $\text{Cr}_2\text{O}_3$  could be formed on the surface of In718 immersed in the LiF-NaK carbonate salt mixture.

However, the high cost of lithium salts is a major obstacle to commercialize this eutectic salt mixture in the CSP industry.

#### 4. Conclusions

Corrosion of SS316, C276, In625 and In718 immersed in three eutectic salt mixtures ( $\text{NaCl-KCl-ZnCl}_2$ ,  $\text{Li}_2\text{CO}_3-\text{Na}_2\text{CO}_3-\text{K}_2\text{CO}_3$  and  $\text{LiF-Na}_2\text{CO}_3-\text{K}_2\text{CO}_3$ ) at 700 °C up to 21 days were experimentally investigated under air atmosphere. The main conclusions are drawn as follows:

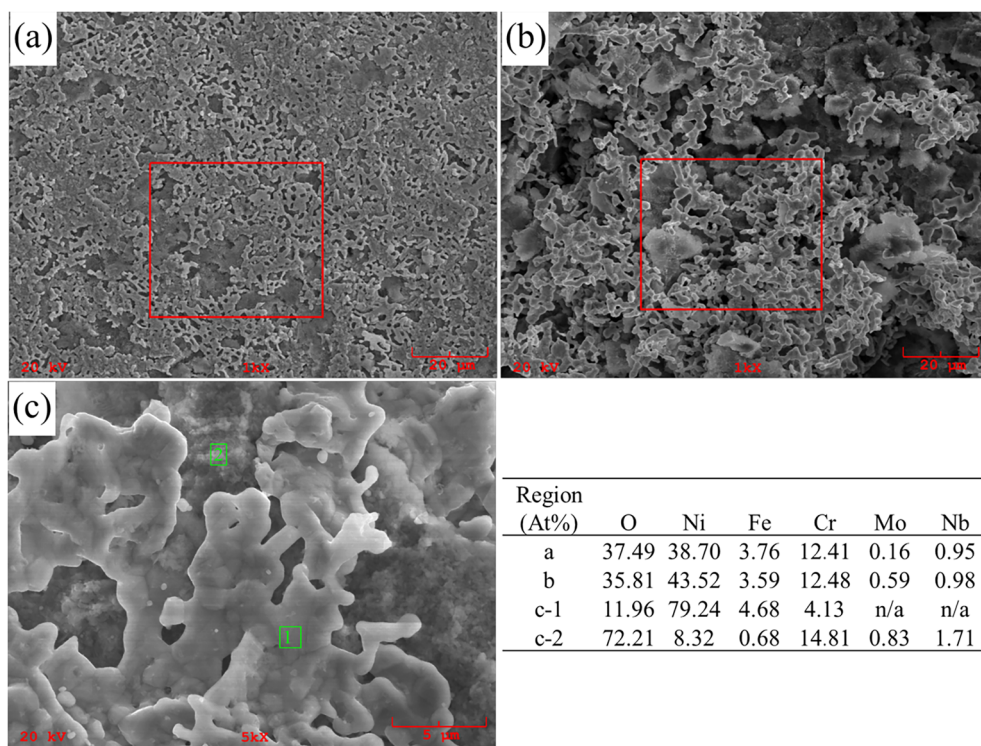


**Fig. 18.** EDS analysis of the In625 coupon immersed in the LiF-NaK carbonate-salt at 700 °C for (a) 7 days, (b) 14 days and (c) 21 days.

**Table 5**  
Corrosion rates of four alloys in three eutectic salt mixtures at 700 °C for 21 days under air atmosphere.

Corrosion rate (μm/year)	SS316	C276	In625	In718
NaKZn chloride-salt	1700	668	447	962
LiNaK carbonate-salt	Mass gain	100	936	146
LiF-NaK carbonate-salt	796 (14 days)	1304	2097	Mass gain (14 days)

- (1) SS316, C276, In625 and In718 all show high corrosion rate (> 450 μm/year) immersed in the NaKZn chloride-salt mixture at 700 °C because of the porous morphology formed on the surfaces of alloys. Although spinel type oxides are the major corrosion products for SS316 and C276, they cannot form a compact layer on the surface of alloys to resist corrosion.
- (2) C276 and In718 show relatively low corrosion rates of 100 and 146 μm/year, respectively, immersed in the LiNaK carbonate-salt mixture for 21 days. In625 has a high corrosion rate of 936 μm/year. Although SS316 shows mass gain after immersion test, it is not corrosion resistant because EDS analysis shows the compositions on the surface is rich in Fe.
- (3) SS316, C276, and In625 all have extremely high corrosion rates immersed in the LiF-NaK carbonate-salt mixture. Although the phases detected by XRD are the same for C276 immersed in the LiF-NaK carbonate-salt and LiNaK carbonate-salt, the corrosion rates show great difference because of different surface morphology as shown in the SEM images. In718 has mass gain instead of mass loss after 21 days immersion. It may be due to the formation of protective oxide layers on the surfaces.

## Acknowledgement

Support from Shenzhen Science and Technology Research and Development Funds (JCYJ20180306171730206, JCYJ20170413105740689) is gratefully acknowledged.

## References

- An, X., Cheng, J., Zhang, P., Tang, Z., Wang, J., 2016. Determination and evaluation of the thermophysical properties of an alkali carbonate eutectic molten salt. *J. Faraday Discuss.* 190, 327–338.
- ASTM G1-03, 2011. Standard Practice for Preparing, Cleaning, and Evaluating Corrosion Test Specimens, 20030.10.
- Bauer, T., Pfleger, N., Breidenbach, N., Eck, M., Laing, D., KAESCHE, S., 2013. Material aspects of solar salt for sensible heat storage. *J. Appl. Energy* 111, 1114–1119.
- Coyle, R., Thomas, T., Lai, Y.G., 1986. Exploratory corrosion tests on alloys in molten salts at 900 °C. *J. Mater. Energy. Syst.* 7, 345–354.
- Ding, W., Shi, H., Xiu, Y., Bonk, A., Weisenburger, A., Jianu, A., Bauer, T., 2018. Hot corrosion behavior of commercial alloys in thermal energy storage material of molten MgCl<sub>2</sub>-KCl-NaCl under inert atmosphere. *Sol. Energy. Mater. Sol. Cells.* 184, 22–30.
- Dorcheh, A.S., Durham, R.N., Galetz, M.C., 2016. Corrosion behavior of stainless and low-chromium steels and IN625 in molten nitrate salts at 600 °C. *J. Sol. Energy. Mater. Sol. Cells.* 144, 109–116.
- Ejima, T., Sato, Y., Yamamura, T., Tamai, K., Hasebe, M., Bohn, M.S., Janz, G.J., 1987. Viscosity of the eutectic Li<sub>2</sub>CO<sub>3</sub>-Na<sub>2</sub>CO<sub>3</sub>-K<sub>2</sub>CO<sub>3</sub> melt. *J. Chem. Eng. Data* 32, 180–182.
- Fernandez, A.G., Rey, A., Lasanta, I., Mato, S., Brady, M.P., Perez, F.J., 2014. Corrosion of alumina-forming austenitic steel in molten nitrate salts by gravimetric analysis and impedance spectroscopy. *J. Mater. Corros.-Werkstoffe. Und. Korrosion* 65, 267–275.
- Goods, S., Bradshaw, R., 2004. Corrosion of stainless steels and carbon steel by molten mixtures of commercial nitrate salts. *J. Mater. Eng. Perform.* 13, 78–87.
- Goods, S., Bradshaw, R., Paririe, M., Chavez, J., 1994. Corrosion of stainless and carbon steels in molten mixtures of industrial nitrates. *J. Sandia. Rep.* 1994–8211.
- Kruizinga, A.M., 2012. Corrosion mechanisms in chloride and carbonate salts. *J. Sandia. Rep.* 2012–7594.
- Kruizinga, A.M., Gill, D.D., Laford, M., McConohy, G., 2013. Corrosion of High Temperature Alloys in Solar Salt at 400, 500, and 680 °C. SANDIA National Laboratories, Albuquerque.
- Kuravi, S., Trahan, J., Goswami, D.Y., Rahman, M.M., Stefanakos, E.K., 2013. Thermal energy storage technologies and systems for concentrating solar power plants. *J. Prog. Energy. Combust. Sci.* 39, 285–319.
- Li, P., Molina, E., Wang, K., Xu, X., Dehghani, G., Kohli, A., Hao, Q., Kassaee, M.H., Jeter, S.M., Teja, A.S., 2016. Thermal and transport properties of NaCl-KCl-ZnCl<sub>2</sub> eutectic salts for new generation high-temperature heat-transfer fluids. *J. Sol. Energy. Eng.* 138, 054501.
- Liu, B., Wei, X., Wang, W., Lu, J., Ding, J., 2017. Corrosion behavior of Ni-based alloys in molten NaCl-CaCl<sub>2</sub>-MgCl<sub>2</sub> eutectic salt for concentrating solar power. *J. Sol. Energy. Mater. Sol. Cells.* 170, 77–86.
- Liu, M., Zheng, J., Lu, Y., Li, Z., Zou, Y., Yu, X., Zhou, X., 2013. Investigation on corrosion behavior of Ni-based alloys in molten fluoride salt using synchrotron radiation techniques. *J. Nucl. Mater.* 440, 124–128.
- Liu, S., Liu, Z., Wang, Y., Tang, J., 2014. A comparative study on the high temperature corrosion of TP347H stainless steel, C22 alloy and laser-cladding C22 coating in

- molten chloride salts. *J. Corros. Sci.* 83, 396–408.
- Olivares, R.I., Chen, C., Wright, S., 2012. The thermal stability of molten lithium-sodium-potassium carbonate and the influence of additives on the melting point. *J. Sol. Energy. Eng.* 134, 041002.
- Olson, L., Ambrosek, J., Sridharan, K., Anderson, M., Allen, T., 2009. Materials corrosion in molten LiF-NaF-KF salt. *J. Fluorine. Chem.* 130, 67–73.
- Olson, L.C., 2009. Materials Corrosion in Molten LiF-NaF-KF Eutectic Salt. PhD dissertation. University of Wisconsin-Madison.
- Peng, Q., Ding, J., Wei, X., Yang, J., Yang, X., 2010. The preparation and properties of multi-component molten salts. *Appl. Energy* 87, 2812–2817.
- Vignarooban, K., Pugazhendhi, P., Tucker, C., Gervasio, D., Kannan, A.M., 2014. Corrosion resistance of hastelloys in molten metal-chloride heat-transfer fluids for concentrating solar power applications. *J. Solar. Energy* 103, 62–69.
- Vignarooban, K., Xu, X., Arvay, A., Hsu, K., Kannan, A.M., 2015. Heat transfer fluids for concentrating solar power systems – A review. *J. Appl. Energy* 146, 383–396.
- Wang, T., Mantha, D., Reddy, R.G., 2015. Novel high thermal stability LiF-Na<sub>2</sub>CO<sub>3</sub>-K<sub>2</sub>CO<sub>3</sub> eutectic ternary system for thermal energy storage applications. *J. Sol. Energy. Mater. Sol. Cells.* 140, 366–375.
- Xu, X., Guo, P., Liu, W., Yang, W., 2017. Entropy generation and Carnot efficiency comparisons of high temperature heat transfer fluid candidates for CSP plants. *J. Int. J. Hydrogen Energy* 42, 20316–20323.
- Xu, X., Vignarooban, K., Xu, B., Hsu, K., Kannan, A.M., 2016. Prospects and problems of concentrating solar power technologies for power generation in the desert regions. *J. Renew. Sustain. Energy. Rev.* 53, 1106–1131.
- Zhang, H.L., Baeyens, J., Degreve, J., Caceres, G., 2013. Concentrated solar power plants: review and design methodology. *J. Renew. Sustain. Energy. Rev.* 22, 466–481.
- Zhao, Z.Y., Chen, Y.L., Thomson, J.D., 2017. Levelized cost of energy modeling for concentrated solar power projects: a China study. *J. Energy* 120, 117–127.
- Zhu, Z., Zhang, D., Mischke, P., Zhang, X., 2015. Electricity generation costs of concentrated solar power technologies in China based on operational plants. *J. Energy* 89, 65–74.